Journal of Materials Chemistry B

ROYAL SOCIETY OF CHEMISTRY

PAPER

View Article Online
View Journal | View Issue

Cite this: J. Mater. Chem. B, 2021, 9, 9383

Development of a novel chromophore reaction-based fluorescent probe for biogenic amines detection†

Lingyun Wang, *[a] Shuqi Xin,[a] Chufeng Zhang,[a] Xueguang Ran,*[b] Hao Tang [a] and Derong Cao [a]

Received 17th August 2021,
Accepted 15th October 2021

DOI: 10.1039/d1tb01791h

rsc.li/materials-b

Biogenic amines (BAs) are important biomarkers to monitor meat spoilage. However, the design of efficient BA fluorescent probes with distinct colorimetric and ratiometric fluorescent dual-channels is still a critical challenge because of similar chemical properties and basicity between BAs and other amines. Herein, pyrrolopyrrole cyanine (**PPCy-1**) is reported to display distinctly high reactivity toward BAs through an ultrasensitive irreversible chromophore reaction for the first time. The reaction mechanism is ascribed to synergistic aza-Michael addition and B–N detachment, followed by hydrolysis to produce low-conjugated diketopyrrolopyrrole and heteroaromatic acetonitrile compounds. As a result, colorimetric and ratiometric fluorescent dual-channel ($\Delta\lambda_{ab}$ = 188 nm and $\Delta\lambda_{em}$ = 151 nm) signals and a limit of detection up to 62.1 nM level for BA solution are acquired. In addition, the colorimetric detection of volatile amine vapor using the **PPCy-1**-loaded filter paper, showing a color change from green to yellow, is feasible. A simple and cost-effective fluorescence "turn on" method using the filter paper or the CAD-40 resin loaded with **PPCy-1** to detect TVB (total volatile bases) originating from shrimp spoilage is further demonstrated.

1. Introduction

Reaction-based fluorescent probes have attracted considerable attention in recent years due to their high selectivity and sensitivity.[1] Among them, the chromophore reaction based fluorescent probe is attractive because the chromophore core is destroyed by an analyte attack, resulting in the loss of π-conjugation and drastic changes of optical properties.[2] So, the chromophore reaction-based probes exhibit superior advantages such as a large shift in UV-vis and emission spectra, and colorimetric and fluorescence dual signals by through a naked-eye visualization process.[3] To date, several chromophore cores such as rhodamines and boron dipyrromethene (BODIPY) have been used as probes to detect GSH, bases and anions.[4–7] Recently, our previous work demonstrated that pyrrolopyrrole aza-BODIPY (PPAB) and lactam-fused aza-BODIPY can undergo a chromophore reaction to generate much smaller conjugated molecules in the presence of amines.[8] In these cases, a high concentration of the probe or long reaction time is needed in order to accelerate the reaction rate, which seriously limits their practical application.

As we know, biogenic amines (BAs) including cadaverine (1,5-pentanediamine), putrescine (1,4-butanediamine), spermidine and spermine mostly exist in the spoiling process of foods, such as meat, fish, seafood, *etc.*[9,10] For instance, cadaverine and putrescine have a bad odor during meat decomposition and are important biomarkers for meat spoilage. In addition, BAs also have a negative effect on human health and physiological functions. The high levels of BAs in spoiled foods are harmful to the central nervous system.[11–13] BAs can react with nitrites to generate nitrosamines, a known carcinogen. Owing to their toxic nature, the real-time monitoring of BA concentration is important and urgent for ensuring public health and food safety. Several reaction-based fluorescent BA probes such as nucleophilic addition, aza-Michael addition, dechlorination and condensation reaction, Schiff base formation, ester aminolysis, and others have been developed.[14] However, the selectivity and sensitivity of existing probes for BA detection still need to be improved for facile and on-site practical use. It is urgent to develop a more efficient chromophore reaction for BA detection.

[a] Key Laboratory of Functional Molecular Engineering of Guangdong Province, School of Chemistry and Chemical Engineering, South China University of Technology, 381 Wushan Road, Guangzhou, 510641, China. E-mail: lingyun@scut.edu.cn

[b] Institute of Animal Science, Guangdong Academy of Agricultural Sciences, Ministry of Agriculture Key Laboratory of Animal Nutrition and Feed Science in South China, State Key Laboratory of Livestock and Poultry Breeding, Guangzhou, 510641, China. E-mail: rxg59@aliyun.com

† Electronic supplementary information (ESI) available. See DOI: 10.1039/d1tb01791h

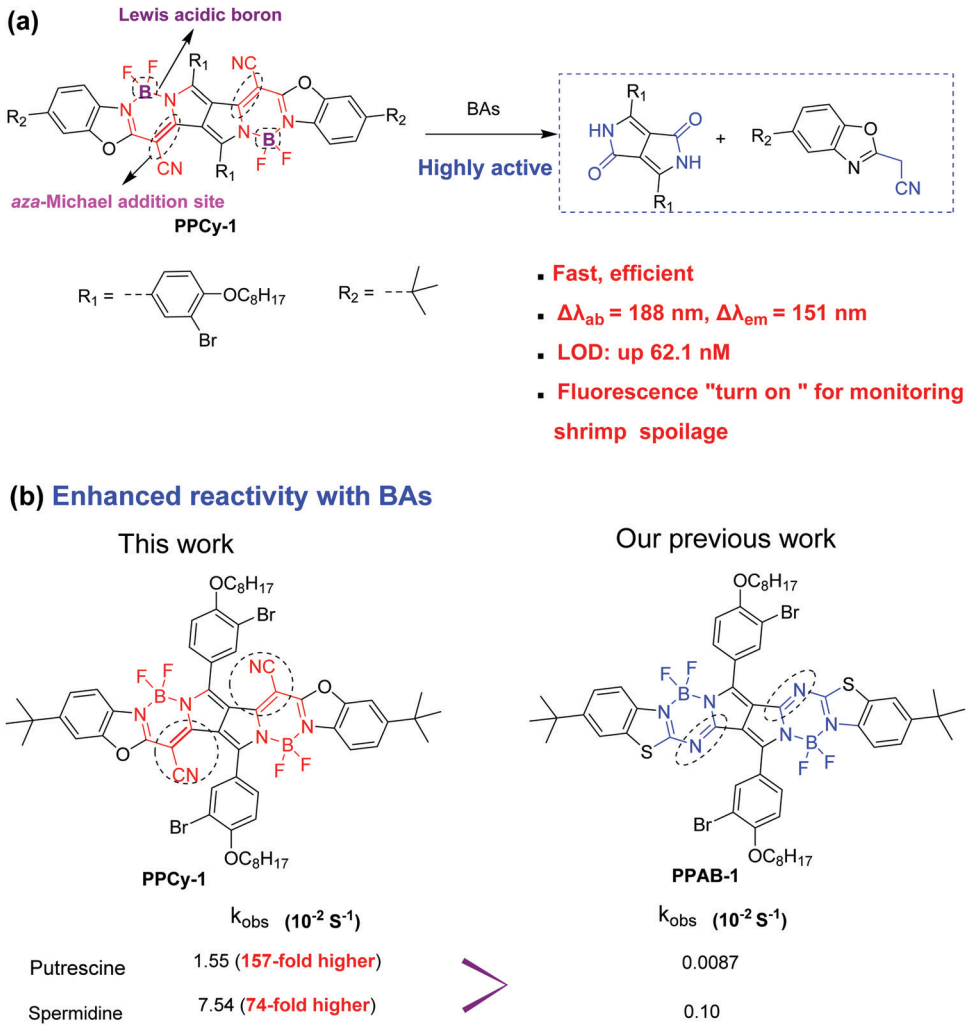

Scheme 1 The chemical structures of **PPCy-1** and **PPAB-1** for BA detection in this work.

Considering the weak nucleophilicity of amines and low BA concentrations in spoiled food, however, it would be more challenging.

To achieve this aim, we herein report a novel and highly efficient chromophore reaction for BA detection with excellent selectivity and sensitivity. The design principle of the probe is as follows: (1) the aza-Michael addition between amine and electrophile could proceed smoothly and rapidly under mild conditions.[15] α,β-Unsaturated nitrile moieties are introduced as amine sensing recognition sites. (2) The Lewis acidic boron center is selected as another reaction site, because the interaction between the boron and nitrogen atoms of amines would reduce the probe's conjugation length. (3) Multiple boron atoms and unsaturated nitrile moieties are integrated into a fluorescent probe. It would be helpful to accelerate the reaction between BAs (with multiple amino groups) and the probe. Based on these considerations, the as-synthesized **PPCy-1** (Scheme 1a) rapidly showed synchronous colorimetric and fluorescence changes ($\Delta\lambda_{ab}$ = 188 nm and $\Delta\lambda_{em}$ = 151 nm) in the presence of BAs within 1 min. More importantly, **PPCy-1** showed 158-fold faster pseudo-first-order rate constants (k_{obs}) with putrescine than our previously used compound **PPAB-1** (Scheme 1b), which strongly indicated that **PPCy-1** was indeed an efficient chromophore reaction-based probe for BA detection. In addition, practical applications in monitoring TVB (total volatile bases) from shrimp spoilage based on a **PPCy-1**-loaded paper-strip and a CAD-40 resin are investigated.

2. Experimental

Compounds **1** and **2** were prepared according to previously reported methods, respectively.[8,16]

2.1. Experimental procedure for amine detection

A stock solution of **PPCy-1** (0.5 mM) was prepared in chloroform, and a dilute solution (2.5 μM) was placed in 3 mL cuvettes for all measurements. For the titration experiments, amine solutions were also prepared in chloroform. **PPCy-1** (2.5 μM) was incubated with different concentrations of amines at 25 °C for the desired time. Absorption and fluorescence spectral analysis data for individual samples were recorded.

2.2. Detection of BA solution/vapor based on the PPCy-1 loaded filter paper

A volume of 200 μL of chloroform stock solution of **PPCy-1** (10 mM) was drop-casted onto the Whatman filter paper followed by evaporation to dryness. The **PPCy-1** loaded filter paper was exposed to different BA solutions for 2 min, and then the color change in daylight and fluorescence change under 365 nm irradiation were measured using a camera.

For sensing of dilute vapors, the **PPCy-1**-loaded filter paper was kept in a 50 mL airtight container with 2 mL of amine solution for 5 min. Then, the absorption and emission spectra were recorded.

2.3. Pretreatment of macroporous CAD-40 resins

Macroporous CAD-40 resins were acquired from Zhengzhou Hecheng New Materials Technology Co., Ltd, China. The resins were soaked in 95% (v/v) aqueous ethanol solution for 24 h and then washed with deionized water for the removal of ethanol. After this, the resins were soaked in 5% solution of HCl for 4 h, then neutralized by washing with deionized water, again soaked in 5% solution of NaOH for 4 h and finally again neutralized by washing with deionized water. Then, the resins were dried and immediately stored in vacuum sealed nylon bags at 4 °C before use.

2.4. Detection of shrimp freshness based on the PPCy-1 loaded filter paper

Fresh shrimp was purchased from the local market. It was sealed with aluminum foil at 28 °C or −4 °C in the presence of the **PPCy-1** loaded filter paper. Pictures were then taken at the desired time under daylight and 365 nm irradiation.

2.5. Detection of shrimp freshness based on the PPCy-1 loaded CAD-40 resin

After pretreatment, the CAD-40 resin (1 g) was immersed in 4 mL of **PPCy-1** chloroform solution (10 mM). After 10 minutes, the CAD-40 resin was collected by filtration and dried at 50 °C for 6 hours. Fresh shrimp was purchased from the local market. It was sealed with aluminum foil at 28 °C or 4 °C in the presence of the **PPCy-1** loaded CAD-40 resin. Pictures were then taken at the desired time under daylight and 365 nm irradiation.

2.6. Synthesis of PPCy-H

Compound **2** (700 mg, 1 mmol), compound **1** (750 mg, 3.5 mmol) and 40 mL of *o*-dichlorobenzene were heated to reflux under nitrogen. Phosphoryl chloride (0.75 mL, 8 mmol) was then added. The reaction was monitored by thin layer chromatography. Once compound **2** was consumed, the reaction was stopped. The reaction solution was cooled to room temperature and a large amount of methanol was added to precipitate a solid, which was filtered and washed with methanol until the filtrate was colorless. The crude product was purified by column chromatography using dichloromethane as the mobile phase. Then, the resulting solids were recrystallized with methanol and dichloromethane to obtain 323 mg **PPCy-H** of blue solid in 29% yield. M.p. > 300 °C. ^{1}H NMR (CD_2Cl_2, 500 MHz) δ 12.31 (d, J = 15.6 Hz, 2H), 7.91–7.84 (m, 2H), 7.72–7.62 (m, 4H), 7.29–7.16 (m, 4H), 7.06 (t, J = 8.6 Hz, 2H), 4.13 (t, J = 6.5 Hz, 4H), 1.87 (m, 4H), 1.53–1.36 (m, 10H), 1.34 (s, 18H), 1.32–1.20 (m, 10H), 0.86 (t, J = 6.2 Hz, 6H). MALDI-TOF (%): calcd for $C_{60}H_{66}Br_2N_6O_4$ 1092.3 found $[M + H]^+$ 1093.1.

2.7. Synthesis of PPCy-1

PPCy-H (250 mg, 0.228 mmol) and *N*,*N*-diisopropylethylamine (2.56 mL, 9.12 mmol) were added to 20 mL of anhydrous dichloromethane at 40 °C under nitrogen. Boron trifluoride ether (0.8 mL, 4.56 mmol) was added and allowed to react for 1 hour. The mixture was cooled to room temperature, washed with saturated $NaHCO_3$ solution, and extracted with dichloromethane. The crude product was purified by column chromatography with the mobile phase (dichloromethane : petroleum ether = 1 : 1). The obtained solid was recrystallized with dichloromethane and methanol to obtain 150 mg **PPCy-1** of green solid in 55% yield. M.p. > 300 °C. ^{1}H NMR (CD_2Cl_2, 500 MHz) δ 7.83 (s, 2H), 7.64 (d, J = 8.4 Hz, 2H), 7.56 (s, 2H), 7.52–7.44 (m, 4H), 7.02 (d, J = 8.9 Hz, 2H), 4.10 (s, 4H), 1.84 (m, 4H), 1.42–1.30 (m, 10H), 1.29 (s, 18H), 1.28–1.12 (m, 10H), 0.85 (t, J = 6.6 Hz, 6H). ^{13}C NMR (CD_2Cl_2, 125 MHz) δ 161.4, 157.8, 155.3, 151.5, 149.4, 146.8, 135.4, 131.5, 131.1, 124.6, 123.3, 122.7, 111.8, 111.8, 111.7, 111.1, 110.8, 69.5, 67.7, 53.9, 53.6, 53.4, 35.3, 31.9, 31.3, 29.3, 29.3, 29.0, 26.0, 22.7, 13.9. MALDI-TOF (%): calcd for $C_{60}H_{64}B_2Br_2F_4N_6O_4$ 1190.6, found $[M]^+$ 1090.6.

2.8. Scanning electron microscopy (SEM)

PPCy-1 (2.5 μM) in chloroform was mixed with 50 μM BAs (putrescine, cadaverine, spermidine, and spermine) at room temperature for 10 min. After drying completely, the sample was observed using a Hitachi S-5000H field emission scanning electron microscope.

3. Results and discussion

3.1. Synthesis

As shown in Scheme S1 (ESI†), **PPCy-H** was prepared by the condensation reaction of diketopyrrolopyrrole (compound **2**) with heteroaromatic acetonitrile (compound **1**) in the presence of phosphoryl chloride. The following reaction between **PPCy-H** and $BF_3{\cdot}Et_2O$ yielded **PPCy-1**. Their chemical structures were characterized by ^{1}H NMR, ^{13}C NMR and MALDI-TOF measurements (Fig. S1–S5, ESI†). The control compound (**PPAB-1**) was also independently prepared (Scheme S1, ESI†). DFT calculations showed that the electron densities of the HOMO and LUMO of **PPCy-1** are mainly located on the conjugated planar PPCy chromophore core and the energy gap was calculated to be 2.025 eV (Fig. S6, ESI†). In addition, **PPCy-1** has good photostability (Fig. S7, ESI†).

3.2. Sensing response of PPCy-1 toward BAs

The response of **PPCy-1** toward typical BAs (putrescine, cadaverine, spermine, and spermidine) at room temperature was monitored (Fig. 1). **PPCy-1** showed two absorption bands at 695/640 nm.

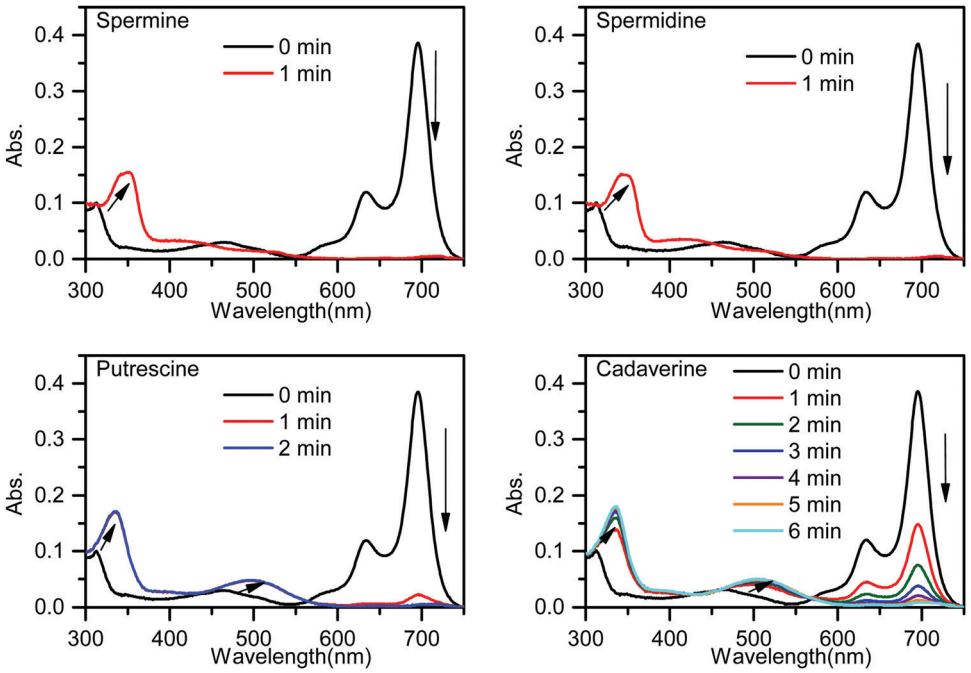

Fig. 1 Time-dependent UV-vis spectra of **PPCy-1** (2.5 μM) in the presence of spermine, spermidine, putrescine and cadaverine (50 μM) at room temperature.

Upon the addition of BAs (50 μM) to a solution of **PPCy-1** (2.5 μM), a distinct color change from green to yellow within 1 min was observed. The time-dependent UV-vis spectra showed that spermine and spermidine had the fastest response, resulting in the disappearance of absorption peaks at 695 and 640 nm, and accompanying the emergence of new peaks at 350 and 425 nm within 1 min. For putrescine and cadaverine, 2 and 5 min were needed to complete the reaction under the same conditions, respectively, where new peaks at 335 and 501 nm were present.

The time-dependent emission spectra indicated that the emission band of **PPCy-1** at 720 nm vanished and the blue-shifted emission (569 nm) appeared immediately (within 1 min) in the presence of spermine and spermidine, resulting in a ratiometric fluorescence response (Fig. 2). Putrescine showed a similar fluorescence response with spermine and spermidine, but with a slightly slower response rate (within 2 min). For cadaverine, more reaction time (more than 10 min) was needed to produce similar emission changes. The disappearance of absorption peaks at 695/640 nm and emission peak at 720 nm implied that the **PPCy-1** chromophore core was destroyed and less conjugated molecules were generated.

The decrease of the absorption peak at 695 nm of **PPCy-1** was linearly proportional to the concentration of BAs (Fig. S8, ESI†). Their limit of detection (LOD) based on a 3σ/slope basis was found to be 0.066, 0.043, 0.229 and 0.179 μM for spermine, spermidine, cadaverine and putrescine, respectively.

3.3. Reactivity and selectivity of PPCy-1 toward various amines

A study of the selectivity and reactivity of **PPCy-1** toward various aliphatic and aromatic amines was investigated by its time-dependent absorption and fluorescence response (Fig. S9 and S10, ESI†). It can be found that the amino number and steric effect of amines play a significant role in determining the reactivity of **PPCy-1** and amine. As shown in Fig. 3a and b, spermine, spermidine, putrescine, cadaverine and 1,3-diaminopropane gave rise to the greatest absorption and fluorescence response. Their decrease at λ_{ab} = 695 nm and λ_{em} = 720 nm was up to 99% within 2 min incubation (entries 2–5). 1,6-Diaminohexane did not induce as strong a spectral response as other diamines; the underlying mechanism was unclear. The absorption decrease at 695 nm and the fluorescence quenching rate at 720 nm were about 20% under the same conditions (entry 6). The primary monoamines, secondary amines, tertiary amines and aromatic amines failed to generate a spectral response (entries 7–20). Meanwhile, other reagents (such as amides, esters, dicarboxylic acids, diols, and alkyl halides) did not elicit any absorption and emission response of **PPCy-1** (data not shown). These results indicated that **PPCy-1** showed excellent selectivity to BA detection. The BA concentration-dependent UV-vis and emission spectra of **PPCy-1** (2.5 μM) in the presence of putrescine, cadaverine, spermidine and spermine at room temperature further indicated the **PPCy-1** chromophore converted into less conjugated compounds, as shown in Fig. S11 and S12 (ESI†). The plots with ratiometric responses indicated that the LOD for spermidine was estimated to be as low as 0.016 μM from the ratiometric change of the absorption intensity simultaneously at 340 and 695 nm. The LOD for other three BAs ranges from 0.033 to 0.084 μM (Fig. S13, ESI†). These results are comparable to the reported ratiometric detection of biogenic diamines using a perylenediimide-based fluoroprobe.[17]

The reaction kinetics between **PPCy-1** and polyamines/diamines (spermidine, spermine, putrescine, 1,3-diaminopropane,

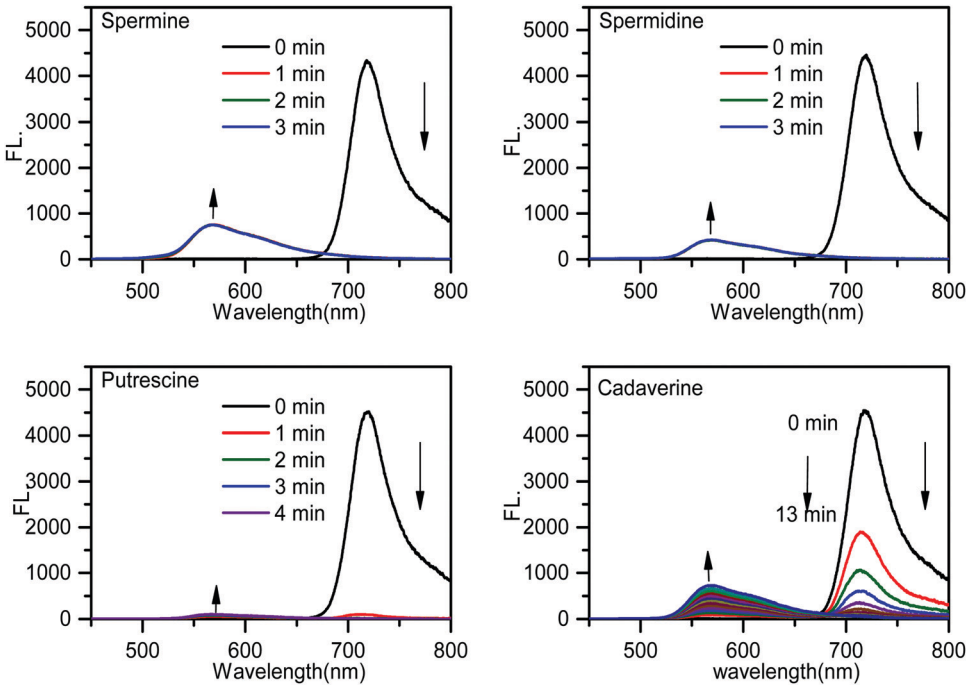

Fig. 2 Time-dependent emission spectra of **PPCy-1** (2.5 μM) in the presence of spermine, spermidine, putrescine and cadaverine (50 μM) at room temperature.

cadaverine, and 1,6-diaminohexane) were investigated. The pseudo-first-order rate constants (k_{obs}) were calculated by monitoring the decrease of absorption bands at 695 nm over time (Fig. 3c). The k_{obs} values of 2.63×10^{-2} s^{-1} and 7.54×10^{-2} s^{-1} for spermine and spermidine were observed, respectively. The diamines showed the k_{obs} values of 0.86×10^{-2}, 1.55×10^{-2}, 0.51×10^{-2}, and 0.16×10^{-2} s^{-1} for 1,3-diaminopropane, putrescine, cadaverine and 1,6-diaminohexane, which was 7.8, 3.9, 13.8, and 46.1-fold lower than that for spermidine, respectively. The reaction rate followed this order: spermidine > spermine > putrescine > 1,3-diaminopropane > cadaverine > 1,6-diaminohexane.

Our previous research indicated that PPAB was also responsive to BAs. So, control experiments with **PPAB-1** were carried out. Spermidine and cadaverine were selected as typical BAs. As shown in Fig. S14 and S15 (ESI†), **PPAB-1** reacted with them in a more awkward way. The k_{obs} values were 0.10×10^{-2} s^{-1} and 0.0087×10^{-2} s^{-1} for spermidine and cadaverine, which was 74- and 157-fold, respectively, lower than that for **PPCy-1**. The detailed data are summarized in Table 1. The results indicated that **PPCy-1** had much higher reactivity than **PPAB-1**. The LOD, sensing characteristics and sensing mechanism as compared with other reported methods are summarized in Table S1 (ESI†), and demonstrate that **PPCy-1** has superior selectivity and sensitivity.

3.4. Detection mechanism study

To investigate the sensing mechanism, we measured the HRMS, ^{1}H, ^{11}B, ^{19}F NMR, and FTIR spectra of **PPCy-1** with an excess of amine. The aza-Michael addition between the amine and electrophile could proceed smoothly and rapidly in a stepwise manner.[15d] In the first step, a tetrahedral intermediate is formed as the consequence of a nucleophilic attack of the amino group on the unsaturated carbon–carbon double bond. Subsequently, the decomposition of the tetrahedral intermediate yields imine (Scheme S2, ESI†). In our case, the multiple reaction was involved between **PPCy-1** and BAs. The reaction mechanism can be ascribed to synergistic aza-Michael addition and B–N detachment, followed by hydrolysis to produce low-conjugated diketopyrrolopyrrole and heteroaromatic acetonitrile compounds (Scheme 2). Taking cadaverine as an amine model compound and based on HRMS, ^{1}H, ^{11}B, ^{19}F NMR, and FTIR spectra, the possible reaction mechanism between **PPCy-1** and cadaverine is shown in Scheme 2. The corresponding intermediate (**IM1–IM5**) and final reaction compounds (**1** and **2**) can be found in the HRMS spectra. As shown in Fig. S16 (ESI†), intermediate **IM1** (1277.7 for $[\mathbf{IM1} + H]^+$) can be found due to the aza-Michael addition reaction that occurs between putrescine and **PPCy-1**. The attack of a B–N bond by another putrescine and decomposition of intermediate **IM1** generated a new BF_2-chelating complex **IM2** (137.0 for $[\mathbf{IM2} + 2H]^+$), heteroaromatic acetonitrile **1** (215.1 for $[\mathbf{1} + H]^+$) and **IM3** (1073.4 for $[\mathbf{IM3}\text{-}C_2H_5]^+$). The following repeated aza-Michael addition and B–N detachment process produced intermediate **IM4** (1073.4 for $[\mathbf{IM4}\text{-}C_2H_5]^+$) and **IM5** (897.4 for $[\mathbf{IM5} + MeOH]^+$). The hydrolysis reaction of **IM5** produced diketopyrrolopyrrole **2**, where the peak at 673.3 was assigned to $[\mathbf{2}\text{-}C_2H_5 + 2H]^+$.

The ^{1}H NMR spectrum of **PPCy-1** in the presence of spermine showed new chemical shifts at 12.45 and 3.83 ppm for N–H of DPP compound **2** and methylene (–CH_2CN) of heteroaromatic acetonitrile **1**, respectively (Fig. 4a). In the ^{11}B NMR

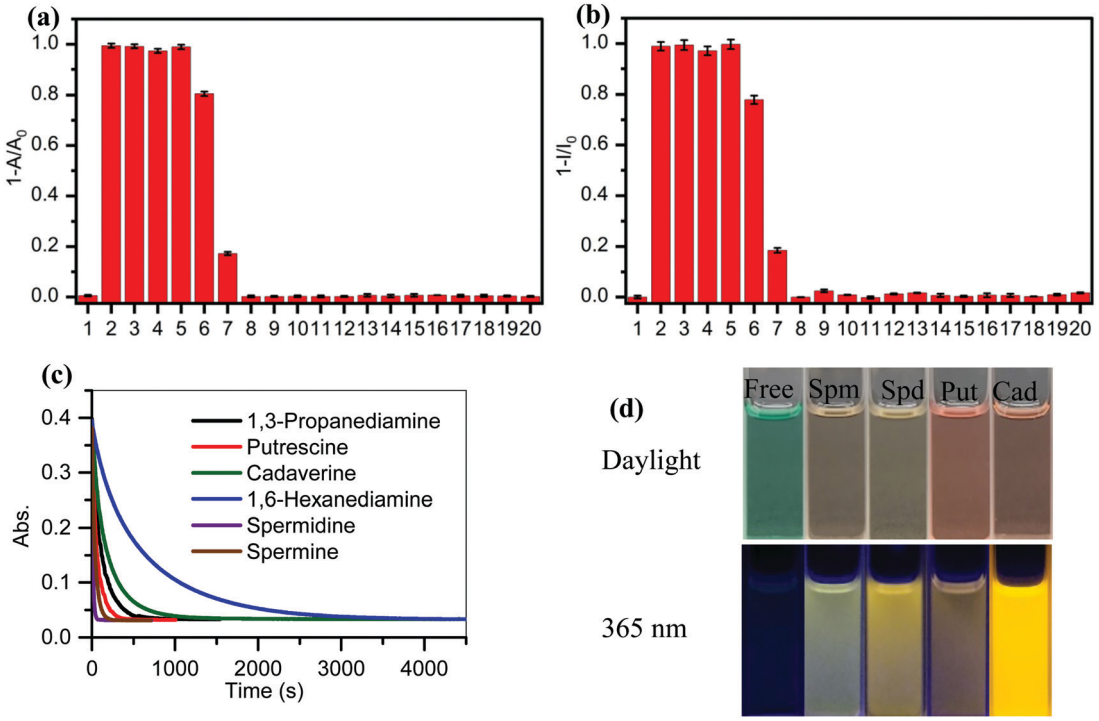

Fig. 3 (a) The absorption at 695 nm and (b) fluorescence changes at 720 nm of **PPCy-1** (2.5 μM) at 25 °C upon the addition of 50 μM of various amines for 2 min (1: blank, 2: spermine, 3: spermidine, 4: 1,3-propanediamine, 5: putrescine, 6: cadaverine, 7: 1,6-hexanediamine, 8: *n*-propylamine, 9: *n*-butylamine, 10: *n*-pentamine, 11: *n*-hexylamine, 12: *n*-heptylamine; 13: *n*-octylamine, 14: cyclohexylamine, 15: aniline, 16: *p*-methoxyaniline, 17: *p*-nitroaniline, 18: trimethylamine, 19: triethylamine, and 20: diethylamine). A_0 and A represent the absorption of **PPCy-1** at 695 nm in the absence and presence of amine, respectively. I_0 and I represent the emission of **PPCy-1** at 720 nm in the absence and presence of amine, respectively. (c) UV-vis kinetics for **PPCy-1** with different BAs at 25 °C at a monitoring wavelength of 690 nm. (d) The photos of PPCy-1 in presence of spermine (Spm), spermidine (Spd), putrescine (Put) and cadaverine (Cad) on daylight and 365 nm irradiation.

Table 1 The pseudo-first-order rate constants (k_{obs}) for the reaction between **PPCy-1** and amines[a]

Amines	Structure	pK_a	k_{obs} ($\times 10^{-2}$ s^{-1})
1,3-Propanediamine	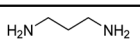	10.94, 9.82	0.86
Putrescine	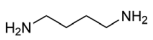	10.80	1.55 0.0087[b]
Cadaverine	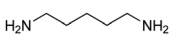	10.05	0.51
1,6-Diaminohexane	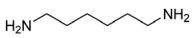	11.85	0.16
Spermidine	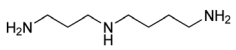	11.56, 10.80, 9.52	7.54 0.10[b]
Spermine	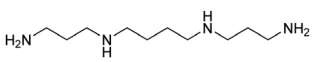	11.50, 10.95, 9.79, 8.90	2.63

[a] Reaction conditions: **PPCy-1** (2.5 μM), amines (50 μM) at room temperature, and incubation time: 2 min. [b] Reaction conditions: **PPAB-1** (2.5 μM), amines (50 μM) at room temperature, and incubation time: 2 min.

and ^{19}F NMR spectra, obvious changes are shown. As shown in Fig. 4b, the triplet at 1.04 ppm and 1.67 ppm in the absence and presence of putrescine was observed, respectively. The two broad peaks at −133.70 and −132.00 ppm shifted to −132.12, −133.51, −135.92 and −136.95 ppm after the addition of spermine (Fig. 4c). The FT-IR spectrum of **PPCy-1** also showed characteristic peaks at 1658 and 3358 cm^{-1}, ascribed to C=O and N–H bonds in DPP compound **2** upon the addition of spermidine (Fig. S17, ESI†). Moreover, the absorption and emission spectra of the reaction mixture are very similar to those of DPP compound **2** and heteroaromatic acetonitrile **1** (Fig. S18 and S19, ESI†). All results indicated that **PPCy-1** underwent a chromophore reaction in the presence of BAs to generate DPP compound **2** and heteroaromatic acetonitrile **1**. The possible mechanism is shown in Scheme 2.

The alkyl chain length, amine group number, basicity and steric hindrance play a synergistic effect on the reaction rate between **PPCy-1** and amine. For 1,6-diaminohexane, the nine-membered B complex formed during the reaction process was not stable, which would delay the reaction rate. So,

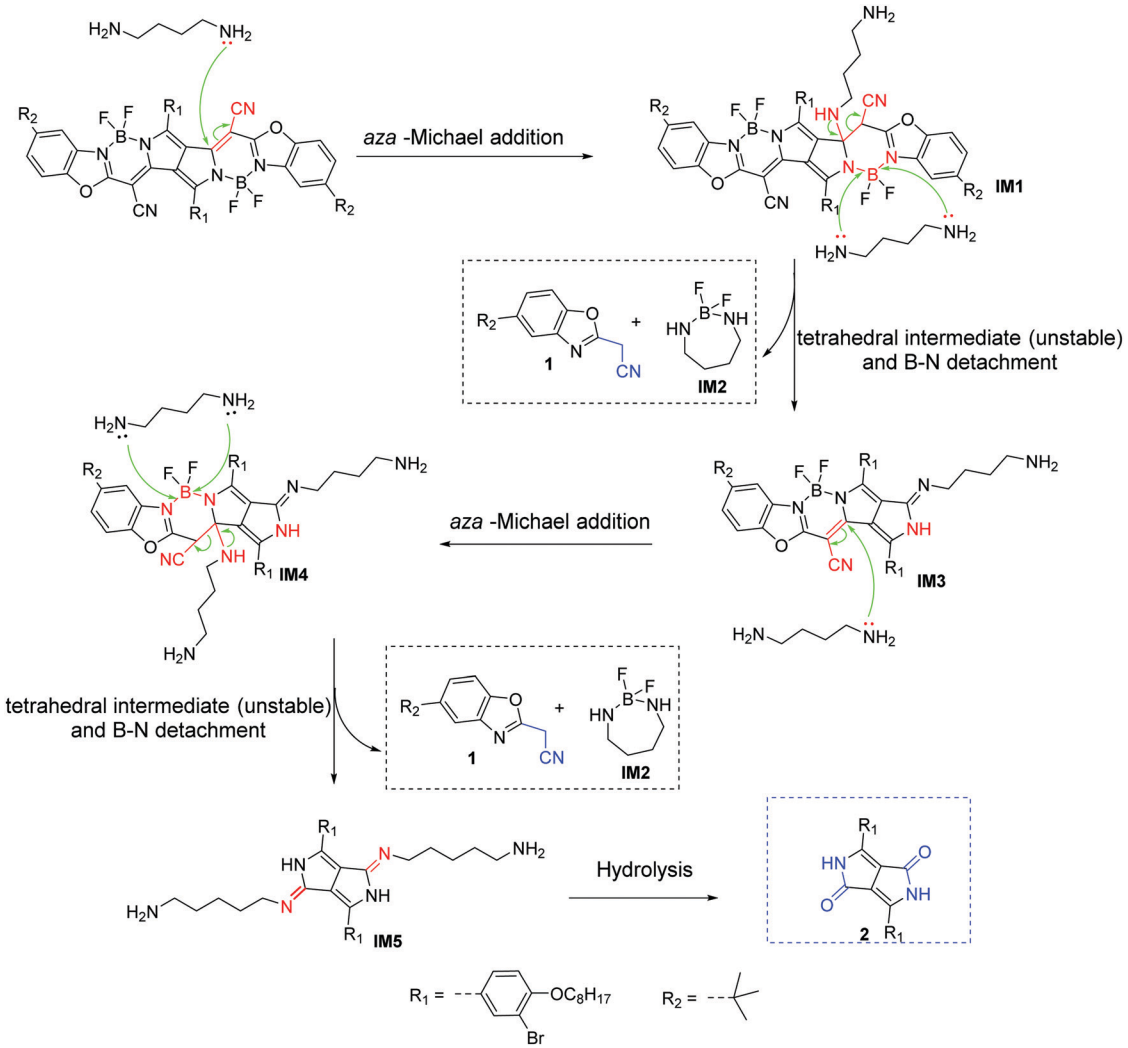

Scheme 2 The possible reaction mechanism between **PPCy-1** and cadaverine.

1,6-diaminohexane has lower pseudo-first-order rate constants (k_{obs}) than other diamines. On the other hand, the amino group number has a positive effect on reactivity. Since spermidine possesses 1.5-fold the amino number than diamine (putrescine, cadaverine, and 1,6-diaminohexane), the former showed a higher reaction rate than the latter. Although spermine has four amino groups, its bulky steric hindrance may be unfavorable to approach and attack **PPCy-1**, resulting in a lower reaction rate than spermidine. Therefore, spermidine showed the highest reaction rate than other BAs.

In addition, the reaction mechanism in Scheme 2 portrays the ultimate products after the reaction of BAs with **PPCy-1**, which are diketopyrrolopyrrole (**2**), heteroaromatic acetonitrile, and chelating complex. Due to the presence of the N–H bond of **2**, various intermolecular H-bonds exist (Fig. S20, ESI†). In particular, intermolecular H-bonds between diketopyrrolopyrrole **2** and amino groups BAs in the presence of an excess of BAs would produce a different aggregation state, which plays an important role in regulating the resulting emission color. As shown in Fig. 5, different surface morphologies are present in the presence of different BAs. These synergistic effects lead to a variation of visible and fluorescence colour in solution in the presence of different BAs (Fig. 3d).

3.5. Application of the PPCy-1-loaded filter paper for BA solution and volatile amine vapor

To further investigate the practical application of **PPCy-1**, the **PPCy-1**-based test strip was used to detect the BA solution. In the presence of a different concentration of BA (spermine, spermidine, putrescine, and cadaverine) solution, a distinct color change was observed both in daylight and under 365 nm irradiation (Fig. 6 and Fig. S21, ESI†). The color changes from green to yellow in daylight and fluorescence "turn on" when increasing amine concentrations were present. Moreover, when the BA solution was used as ink for writing on the **PPCy-1** loaded filter paper, a distinct color change was also observed (Fig. S22, ESI†).

For practical applications, vapor sensing is more convenient and preferable. In this study, some volatile amines, including trimethylamine, triethylamine, putrescine, 1,3-diaminepropane,

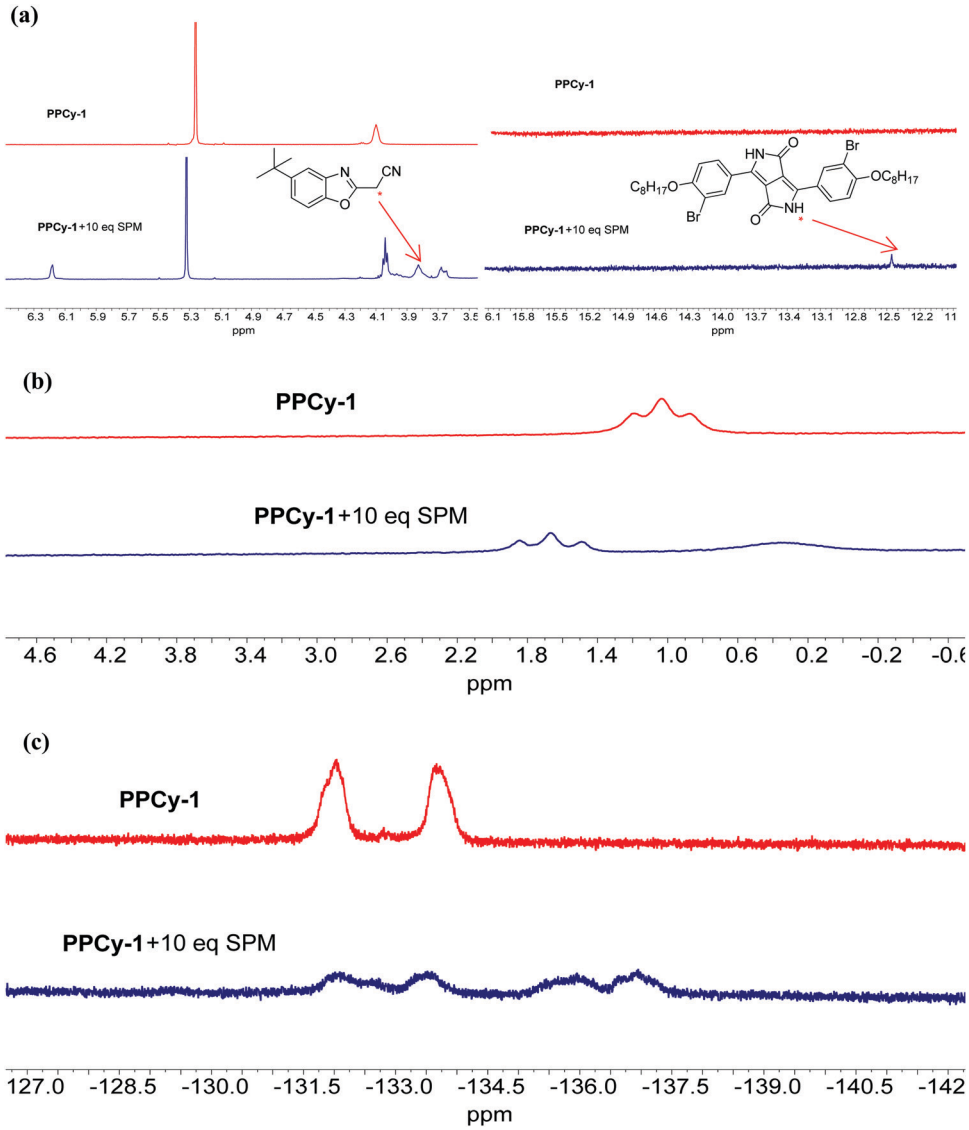

Fig. 4 (a) Partial ^{1}H, (b) ^{11}B and (c) ^{19}F NMR spectra of **PPCy-1** (10 mM) in the presence of spermidine (SPM, 100 mM) in CD_2Cl_2 at room temperature.

cadaverine, spermidine and ammonia, were selected as a typical amine vapor model. **PPCy-1** solution possessed a shoulder absorption at 695/640 nm and an emission at 720 nm by fine structures. However, the **PPCy-1**-loaded filter paper showed multiple broad absorption bands and weak emissive bands, implying strong intermolecular π–π interactions in the aggregated state. After 5 min incubation (trimethylamine, triethylamine, and putrescine vapor), the absorption bands at 701 and 648 nm were largely decreased and two new absorption bands at 508 and 339 nm were present. As a result, the color change from green to yellow can be easily observed by naked eyes, which was consistent with results previously found in solution (Fig. 7). Cadaverine, spermidine and ammonia performed similarly, but did not give as great an absorption change as the former under the same conditions (Fig. S23, ESI†).

The fluorescence enhancement was observed toward trimethylamine, triethylamine, putrescine, 1,3-diaminepropane, cadaverine, and spermidine vapors (Fig. S24, ESI†). The greatest green fluorescence 'turn-on' phenomenon was observed after exposure to ammonia vapor. To obtain insights into this observation, the time-dependent absorption and emission spectra of **PPCy-1** solution in the presence of ammonia vapor were studied. The results were similar with those in the presence of BAs, indicating that ammonia had a similar chromophore reaction mechanism as discussed above (Fig. S25, ESI†).

The intermolecular homogeneous reaction between dispersed **PPCy-1** and BAs is involved in solution. Instead, the heterogeneous reaction between solid **PPCy-1** and gaseous BAs is involved when a **PPCy-1**-based test strip was exposed to volatile amines. The selectivity difference of **PPCy-1** for BAs in solution and solid can arise for many reasons including nucleophilicity, vapor pressure, steric hindrance, relative vapor density and the affinity to the sensing material. It is difficult to disentangle which one is the decisive factor. In our case, it seems that the amines with high vapor pressures and nucleophilicity, and less steric hindrance would be beneficial to accelerate the reaction between amine vapor

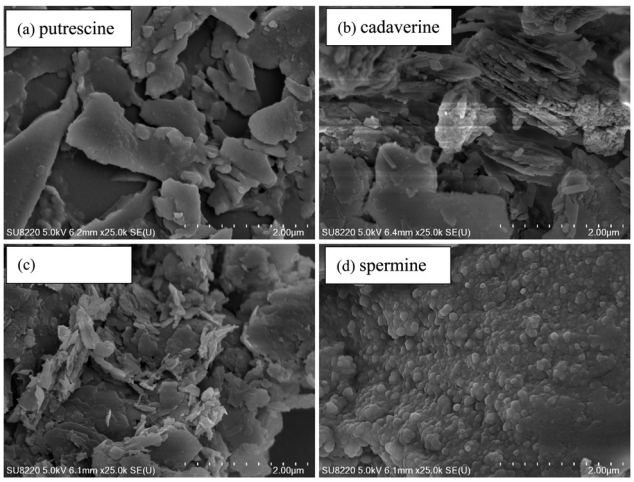

Fig. 5 SEM images of **PPCy-1** (2.5 μM) in the presence of BAs (50 μM).

and solid **PPCy-1**. For example, trimethylamine, ammonia and triethylamine have higher vapor pressures (~214.6, 7.6 and 48 kPa, respectively, Table S2, ESI†), and higher reactivity is obtained. Cadaverine and spermidine possess much lower vapor pressures (0.13 and 0.036 kPa, respectively, Table S2, ESI†) than the former, resulting in slower reactivity and less photophysical changes.

3.6. Detection of TVB (total volatile bases) originating from shrimp spoilage

The sum of primary, secondary, and tertiary amines in the form of volatile amines and toxic nitrogen compounds are classified as TVB (total volatile bases). The compounds have aromatic and heterocyclic structures and include BAs such as putrescine and cadaverine.[18] Moderate levels of BAs are essential and beneficial to regulate physiological activities in the human body. However, there are toxic thresholds for BAs that could lead to a wide range of illnesses including severe headaches, hypertension, abdominal pain, tachycardia, *etc.*[19,20] There have been many research studies investigating the relationship between TVB levels and the freshness of fish and other seafood products.[21] The widespread application of TVB to determine fish freshness has been established.[22]

The potentiality of the **PPCy-1**-loaded filter paper was used to detect TVB for the determination of spoilage in raw shrimp samples. Upon exposure to shrimps in a sealed plastic container, the green fluorescence 'turn-on' responses over 12 h incubation at 4 °C were observed. The fluorescence continued to strengthen with the increase of incubation time. The low background and distinct change from dark to a green color were helpful to provide visual detection with considerable simplicity (Fig. 8a). As a control, when shrimps were stored in the refrigerator at −4 °C or 4 °C, no emission change can be found (Fig. S26, ESI†).

The macroporous CAD-40 resin is an organic adsorbent composed of polystyrene cross-linked with divinylbenzene. It has a suitable particle diameter (0.3–1.25 mm), large surface area (450–500 m^2 g^{-1}) and small average pore diameter (7–8 nm), and is a good candidate for high loading **PPCy-1** and plays a positive role in improving the sensing sensitivity. As shown in Fig. 8b, when the weakly emissive **PPCy-1**-loaded

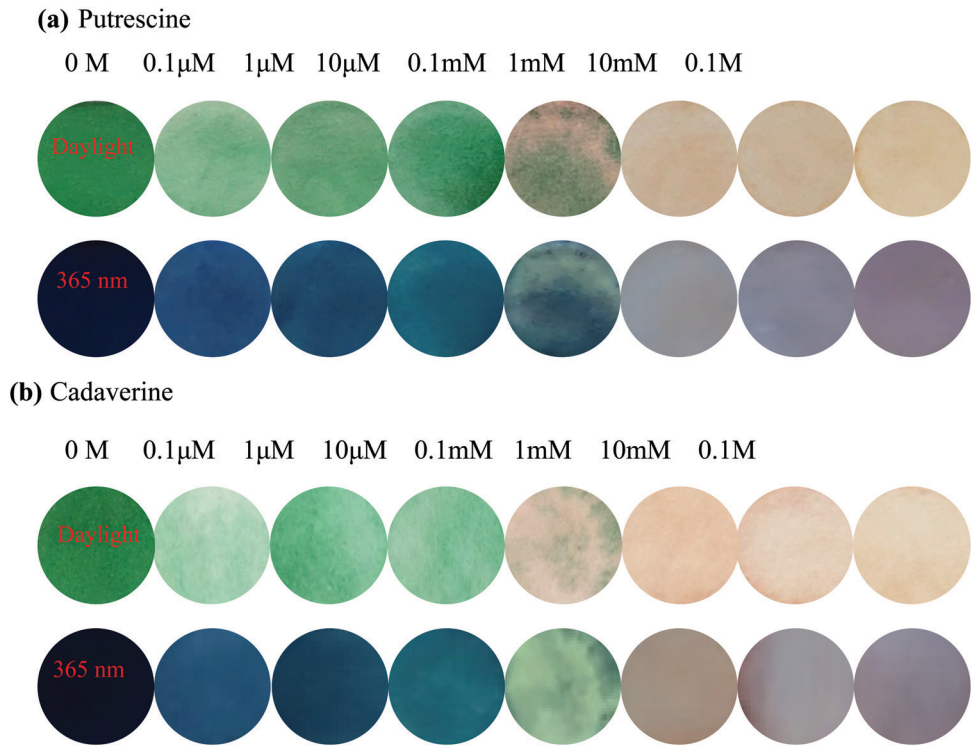

Fig. 6 The color and emission changes of the **PPCy-1**-loaded filter paper with colorimetric (top) and fluorescent (bottom) dual modes in the presence of (a) putrescine and (b) cadaverine solutions at 25 °C.

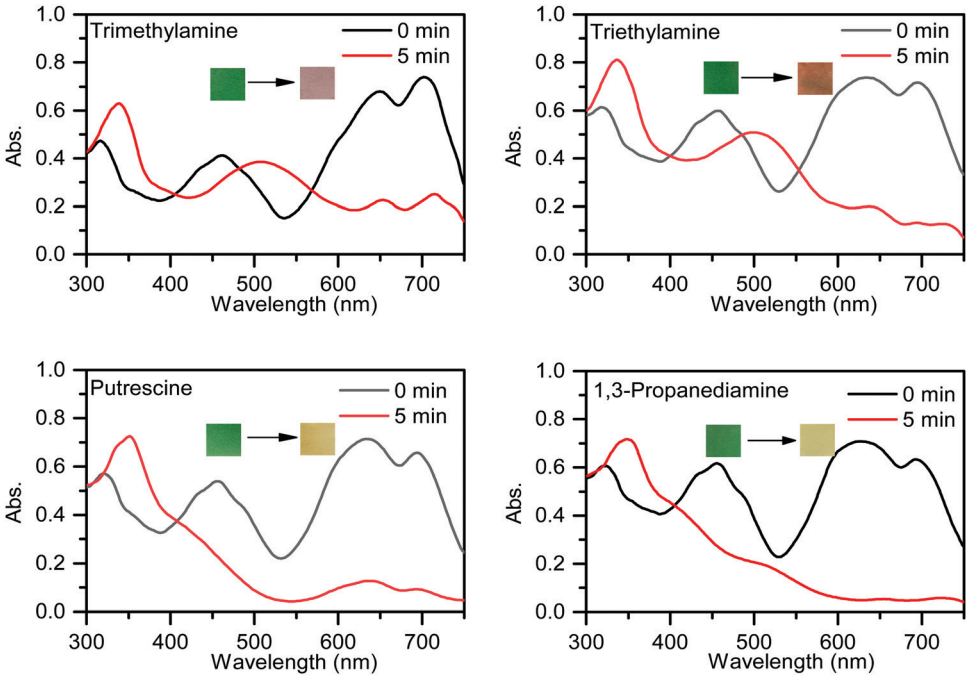

Fig. 7 UV-vis spectra and photos of the **PPCy-1**-loaded filter paper before and after exposure to trimethylamine, triethylamine, putrescine and 1,3-diaminepropane vapor.

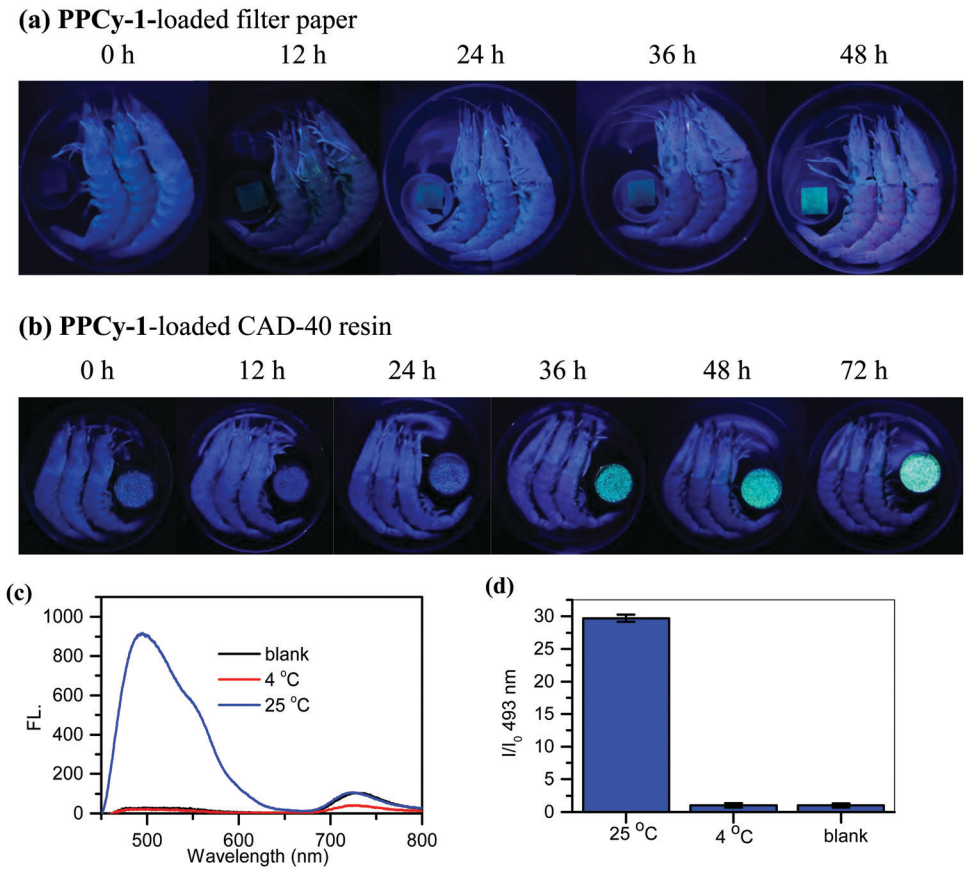

Fig. 8 Monitoring shrimp spoilage at 25 °C by (a) **PPCy-1**-loaded filter paper and (b) **PPCy-1**-loaded CAD-40 resin with fluorescent modes. (c) The emission spectra and (d) I/I_0 at 493 nm of the **PPCy-1**-loaded CAD-40 resin in the absence and presence of shrimp storage at 4 °C and 25 °C for 36 h.

CAD-40 resin was incubated with shrimp at 25 °C for 12 h, a more obvious green fluorescence 'turn-on' response was observed. The new emission peaks at 493 and 549 nm were greatly intensified to yield 30-fold fluorescence enhancement at 493 nm (Fig. 8c and d). The resulting color change was evident to the naked eye under UV irradiation. In contrast, there were no obvious emission changes to shrimps kept in the refrigerator at 4 °C for 72 h (Fig. S27, ESI†).

4. Conclusions

In summary, we report a new chromophore reaction-based signaling mechanism for the construction of a fluorescent probe (**PPCy-1**) for BA detection. **PPCy-1** enriched in the large arsenal of the amine-responsive probe: its reaction with BAs results in 188 nm absorption and 151 nm emission hypsochromic shift signal within 1 min. The high sensitivity and selectivity confer its utility in assessment of food quality, to the industrial/environmental monitoring of volatile amines. To the best of our knowledge, this work is the first example of a PPCy dye conversion to DPP compound through an efficient chromophore reaction for BA detection.

Author contributions

Lingyun Wang contributed to the conception of the study; Shuqi Xin performed the experiment; Chufeng Zhang contributed significantly to analysis; Xueguang Ran performed the data analyses; and Hao Tang and Derong Cao helped in performing the analysis with constructive discussions.

Conflicts of interest

There are no conflicts to declare.

Acknowledgements

We are grateful to the National Natural Science Foundation of China (22071065), the Natural Science Foundation of Guangdong Province (2018B030311008) and the Natural Science Foundation of Guangzhou (201904010414) for financial support.

References

1 (*a*) J. Chan, S. C. Dodani and C. J. Chang, Reaction-based small-molecule fluorescent probes for chemoselective bioimaging, *Nat. Chem.*, 2012, **4**, 973–984; (*b*) A. R. Lippert, E. J. New and C. J. Chang, Reaction-based fluorescent probes for selective imaging of hydrogen sulfide in living cells, *J. Am. Chem. Soc.*, 2011, **133**, 10078–10080; (*c*) D. G. Cho and J. L. Sessler, Modern reaction-based indicator systems, *Chem. Soc. Rev.*, 2009, **38**, 1647–1662.

2 (*a*) J. Yoshino, N. Kano and T. Kawashima, Fluorescence properties of simple N-substituted aldimines with a B–N interaction and their fluorescence quenching by a cyanide ion, *J. Org. Chem.*, 2009, **74**, 7496–7503; (*b*) Y. Yang, S. K. Seidlits, M. M. Adams, V. M. Lynch and J. B. Shear, A highly selective low-background fluorescent imaging agent for nitric oxide, *J. Am. Chem. Soc.*, 2010, **132**, 13114–13116; (*c*) V. Bhalla, H. Singh and M. Kumar, Facile cyclization of terphenyl to triphenylene: a new chemodosimeter for fluoride ions, *Org. Lett.*, 2010, **12**, 628–631.

3 J. J. Du, M. M. Hu, J. L. Fan and X. J. Peng, Fluorescent chemodosimeters using ''mild'' chemical events for the detection of small anions and cations in biological and environmental media, *Chem. Soc. Rev.*, 2012, **41**, 4511–4535.

4 (*a*) H. Liu, S. S. Wang, H. Gao and Z. Shen, Reversible reaction-based fluorescent probes for dynamic sensing and bioimaging, *Eur. J. Org. Chem.*, 2020, 5647–5663; (*b*) L. Y. Wang, X. G. Ran, H. Tang and D. R. Cao, Recent advances on reaction-based amine fluorescent probes, *Dyes Pigm.*, 2021, **194**, 109634.

5 (*a*) A. Morozumi, M. Kamiya, S. Uno, K. Umezawa, R. Kojima, T. Yoshihara, S. Tobita and Y. Urano, Spontaneously blinking fluorophores based on nucleophilic addition/dissociation of intracellular glutathione for live-cell super-resolution imaging, *J. Am. Chem. Soc.*, 2020, **142**, 9625–9633; (*b*) K. Umezawa, M. Yoshida, M. Kamiya, T. Yamasoba and Y. Urano, Rational design of reversible fluorescent probes for live-cell imaging and quantification of fast glutathione dynamics, *Nat. Chem.*, 2017, **9**, 279–286.

6 D. H. Hu, T. Zhang, S. Y. Li, T. J. Yu, X. H. Zhang, R. Hu, J. Feng, S. Q. Wang, T. L. Liang, J. M. Chen, L. N. Sobenina, B. A. Trofimov, Y. Li, J. S. Ma and G. Q. Yang, Ultrasensitive reversible chromophore reaction of BODIPY functions as high ratio double turn on probe, *Nat. Commun.*, 2018, **9**, 362.

7 (*a*) H. Lu, J. Mack, Y. Yang and Z. Shen, Structural modification strategies for the rational design of red/NIR region BODIPYs, *Chem. Soc. Rev.*, 2014, **43**, 4778–4823; (*b*) S. S. Wang, H. Liu, J. Mack, J. G. Tian, B. Zou, H. Lu, Z. F. Li, J. X. Jiang and Z. Shen, *Chem. Commun.*, 2015, **51**, 13389–13392; (*c*) X. Y. Qu, W. T. Song and Z. Shen, A highly selective NIR fluorescent Turn-on probe for hydroxyl radical and its application in living cell images. Frontiers, *Chemistry*, 2019, **7**, 598; (*d*) H. Liu, W. Song, D. Gröninger, L. Zhang, Y. H. Lu, S. K. Chan, Z. K. Zhou, K. Rurack and Z. Shen, Real-time monitoring of newly acidified organelles during autophagy enabled by reaction-based BODIPY dyes, *Commun. Biol.*, 2019, **2**, 442.

8 (*a*) L. Q. Li, W. T. Li, X. G. Ran, L. Y. Wang, H. Tang and D. R. Cao, A highly efficient, colorimetric and fluorescent probe for recognition of aliphatic primary amines based on a unique cascade chromophore reaction, *Chem. Commun.*, 2019, **55**, 9789–9792; (*b*) L. Q. Li, W. T. Li, L. Y. Wang, H. Tang, D. R. Cao and X. G. Ran, Pyrrolopyrrole aza-BODIPY dyes for ultrasensitive and highly selective biogenic diamine detection, *Sens. Actuators, B*, 2020, **312**, 127953; (*c*) L. Y. Wang, H. Ding, H. Tang, D. R. Cao and X. G. Ran, A novel and efficient chromophore reaction based on a lactam-fused aza-BODIPY for polyamine detection, *Anal. Chim. Acta*, 2020, **1135**, 38–46; (*d*) W. T. Li, L. Y. Wang, T. L. Sun, H. Tang, B. Bui, D. R. Cao, R. B. Wang and W. Chen, Characterization of nanoparticles combining

polyamine detection with photodynamic therapy, *Commun. Biol.*, 2021, **4**, 803.

9 Q. Chen, C. Zhang, J. Zhao and Q. Ouyang, Recent advances in emerging imaging techniques for non-destructive detection of food quality and safety, *Trends Anal. Chem.*, 2013, **52**, 261–274.

10 (*a*) D. I. Ellis, V. L. Brewster, W. B. Dunn, J. W. Allwood, A. P. Golovanov and R. Goodacre, Fingerprinting food: current technologies for the detection of food adulteration and contamination, *Chem. Soc. Rev.*, 2012, **41**, 5706–5727; (*b*) A. I. Danchuk, N. S. Komova, S. N. Mobarez, S. Y. Doronin, N. A. Burmistrova, A. V. Markin and A. Duerkop, Optical sensors for determination of biogenic amines in food, *Anal. Bioanal. Chem.*, 2020, **412**, 4023–4036; (*c*) G. Munzi, S. Failla and S. D. Bella, Highly selective and sensitive colorimetric/fluorometric dual mode detection of relevant biogenic amines, *Analyst*, 2021, **146**, 2144–2151.

11 N. Kaur, S. Chopra, G. Singh, P. Raj, A. Bhasin, S. K. Sahoo, A. Kuwar and N. Singh, Chemosensors for biogenic amines and biothiols, *J. Mater. Chem. B*, 2018, **6**, 4872–4902.

12 A. Önal, A review: current analytical methods for the determination of biogenic amines in foods, *Food Chem.*, 2007, **103**, 1475–1486.

13 O. Corduneanu, A. M. Chiorcea-Paquim, V. Diculescu, S. M. Fiuza, M. P. M. Marques and A. M. Oliveira-Brett, DNA interaction with Palladium chelates of biogenic polyamines using atomic force microscopy and voltammetric characterization, *Anal. Chem.*, 2010, **82**, 1245–1252.

14 (*a*) Z. Jiao, Y. Zhang, W. Xu, X. T. Zhang, H. B. Jiang, P. C. Wu, Y. Y. Fu, Q. G. He, H. M. Cao and J. G. Cheng, Highly efficient multiple-anchored fluorescent probe for the detection of aniline vapor based on synergistic effect: chemical reaction and PET, *ACS Sens.*, 2017, **2**, 687–694; (*b*) C. Bao, S. F. Shao, H. F. Zhou and Y. F. Han, A new ESIPT-based fluorescent probe for the highly sensitive detection of amine vapors, *New J. Chem.*, 2021, **45**, 10735–10740; (*c*) S. Mallick, F. Chandra and A. L. Koner, A ratiometric fluorescent probe for detection of biogenic primary amines with nanomolar sensitivity, *Analyst*, 2016, **141**, 827–831; (*d*) A. R. Longstreet, M. J. R. R. Chandler, K. Hanson, N. Zhan, J. J. Hrudka, H. Mattoussi, M. Shatruk and D. T. McQuade, Ylidenemalononitrile enamines as fluorescent ''Turn-On'' indicators for primary amines, *J. Am. Chem. Soc.*, 2014, **136**, 15493–15496; (*e*) J. V. Ros-Lis, M. D. Marcos, R. Mártinez-Máez, K. Rurack and J. Soto, A regenerative chemodosimeter based on metal-induced dye formation for the highly selective and sensitive optical determination of Hg^{2+} ions, *Angew. Chem., Int. Ed.*, 2010, **44**, 4405–4407; (*f*) B. T. Zhu, L. R. Jiang, T. H. Chen, G. M. Bao, L. T. Zeng, X. C. Hu and H. Q. Yuan, A colorimetric and fluorescence lighting-up probe for the determination of biogenic primary diamine during the spoilage of fish, *Dyes Pigm.*, 2021, **186**, 108963; (*g*) L. Y. Wang, X. G. Ran, H. Tang and D. R. Cao, Recent advances on reaction-based amine fluorescent probes, *Dyes Pigm.*, 2021, **194**, 109634.

15 (*a*) C. D. Hurd and J. Patterson, The addition of hydroxylamine to ω-nitrostyrene, furylnitroethylene and nitroolefins, *J. Am. Chem. Soc.*, 1953, **75**, 285–288; (*b*) Y. Y. Ku, R. R. Patel, B. A. Roden and D. P. Sawick, Synthesis of substituted heterocycles. Simple method for the introduction of the n-hydroxyurea functionality, *Tetrahedron Lett.*, 1994, **35**, 6017–6020; (*c*) I. Panfil, C. Bełzecki, M. Chmielewski and K. Suwińska, Reaction of α,β-unsaturated sugar lactones with formaldoxime, *Tetrahedron*, 1989, **45**, 233–238; (*d*) M. G. Vinogradov, O. V. Turova and S. G. Zlotin, Recent advances in the asymmetric synthesis of pharmacology-relevant nitrogen heterocycles via stereoselective aza-Michael reactions, *Org. Biomol. Chem.*, 2019, **17**, 3670–3708.

16 (*a*) S. Wiktorowski, C. Rosazza, M. J. Winterhalder, E. Daltrozzo and A. Zumbusch, Water-soluble pyrrolopyrrole cyanine (PPCy) NIR fluorophores, *Chem. Commun.*, 2014, **50**, 4755–4758; (*b*) G. M. Fischer, A. P. Ehlers, A. Zumbusch and E. Daltrozzo, Near-infrared dyes and fluorophores based on diketopyrrolopyrroles, *Angew. Chem., Int. Ed.*, 2010, **46**, 3750–3753.

17 R. Roy, N. R. Sajeev, V. Sharma and A. L. Koner, Aggregation induced emission switching based ultrasensitive ratiometric detection of biogenic diamines using a perylenediimide-based smart fluoroprobe, *ACS Appl. Mater. Interfaces*, 2019, **11**, 47207–47217.

18 (*a*) F. Saleem, B. N. Ametaj, S. Bouatra, R. Mandal, Q. Zebeli and S. M. Dunn, A metabolomics approach to uncover the effects of grain diets on rumen health in dairy cows, *J. Dairy Sci.*, 2012, **95**, 6606–6623; (*b*) H. Li, Q. Chen, J. Zhao and M. Wu, Nondestructive detection of total volatile basic nitrogen (TVB-N) content in pork meat by integrating hyperspectral imaging and colorimetric sensor combined with a nonlinear data fusion, *LWT–Food Sci. Technol.*, 2015, **63**, 268–274.

19 F. Ozcelik, M. C. Temel, I. K. Ozcelik, E. Kale and M. S. Sankhla, The role of biogenic amines in nutrition toxicology: review, *Int. J. Nutr.*, 2020, **5**, 21–29.

20 D. Erdag, O. Merhan and B. Yildiz, Biochemical and pharmacological properties of biogenic amines, in *Biogenic Amines*, ed. C. Proestos, 2019, https://www.intechopen.com/books/biogenic-amines.

21 (*a*) P. Howgate, A critical review of total volatile bases and trimethylamine as indices of freshness of fish. Part 2. Formation of the bases, and application in quality assurance, *Electron. J. Environ., Agric. Food Chem.*, 2010, **9**, 58–88; (*b*) P. Y. Hamaguchi, W. Y. Weng, T. Kobayashi, J. Runglertkreigkrai and M. Tanaka, Effect of fish meat quality on the properties of biodegradable protein films, *Food Sci. Technol. Res.*, 2007, **13**, 200–204; (*c*) L. Shi, T. Yin, L. Wang, G. Xiong, R. Gao, A. Ding and C. Jiao, Effect of prechilling time on the physicochemical properties of channel catfish during frozen storage, *Int. J. Refrig.*, 2020, **115**, 56–62; (*d*) X. Xiong, B. He, D. Jiang, X. Dong, C. Yu and H. Qi, Postmortem biochemical and textural changes in the sea cucumber Stichopus japonicus body wall (SJBW) during iced storage, *LWT--Food Sci. Technol.*, 2020, **118**, 108705.

22 A. A. Bekhit, B. Holman, S. G. Giteru and D. L. Hopkins, Total volatile basic nitrogen (TVB-N) and its role in meat spoilage: A review, *Trends Food Sci. Technol.*, 2021, **109**, 280–302.

